Desalination and Water Treatment
www.deswater.com

doi: 10.5004/dwt.2022.28044

247 (2022) 28–39
January

Pressure drop across membrane spacer-filled channels using porous media characteristics and computational fluid dynamics simulation

Bassel A. Abdelkader, Mostafa H. Sharqawy*

School of Engineering, College of Engineering and Physical Sciences, University of Guelph, 50 Stone Rd E, Guelph, Ontario, N1G 2W1 Canada, Tel. +1 (519) 824-4120 Ext. 58973; emails: babdelka@uoguelph.ca (B.A. Abdelkader), melsharq@uoguelph.ca (M.H. Sharqawy)

Received 24 July 2021; Accepted 11 December 2021

ABSTRACT

The presence of spacers in membrane modules generates turbulence which enhances the mass transfer through the membrane. However, spacers increase the pressure drop in the flow channels which increases the operating cost. Previous approaches used empirical correlations to estimate the pressure drop across spacer-filled channels in membrane modules. In this study, a different approach is proposed for accurate pressure drop prediction by treating the spacer as a porous media and using Darcy–Forchheimer's model for flow in porous media. The pressure drop is predicted using Darcy–Forchheimer's model and computational fluid dynamics simulation which is validated using experimental data available in the literature. This study focuses on the effect of spacer filament diameter and porosity on the permeability coefficient, and pressure drop. The critical Reynolds number is calculated to identify the transition between Darcy and non-Darcy flow through the spacer-filled channels. It is found that the permeability coefficient increases with the spacer filament diameter and porosity. This study also proposes a correlation to calculate the permeability coefficient based on the spacer porosity and filament diameter.

Keywords: Membrane spacer; Pressure drop; Porous media; Computational fluid dynamics simulation

1. Introduction

Membrane spacers are critical components of flat plate and spiral wound membrane modules, which affect the pressure drop, mass transfer, and concentration distribution across the flow channels [1–3]. These spacers generate turbulence within the vicinity of the membrane's active layer, thus, promoting mixing which decreases concentration polarization and enhances the mass transfer through the membrane [4–7]. Using a membrane spacer was shown to increase the mass flux up to 5 times greater than without a spacer [8,9]. However, a drawback of adding membrane spacers is the significant increase of pressure drop across the channel, which increases the operational cost of the membrane module [10–13].

The increase in pressure drop caused by spacers was investigated in previous studies [8–16]. Haidari et al. [10] found that spacers increase the pressure drop by 2–8.5 times compared to an empty channel depending on the properties of the spacer. Similarly, Kavianipour et al. [11] reported that a spacer-filled channel generates a pressure drop five times greater than an unobstructed channel. Even though using a membrane spacer increases pressure drop, it is still practical to use it as the increase of mass flux is more important to the performance compared with the increase in pumping power [8,14,15]. Thus, the effect of spacers should be taken into consideration when designing and modeling membrane modules to obtain accurate performance results.

The pressure drop through spacer-filled channels has been investigated experimentally for several spacer

* Corresponding author.

geometries and empirical correlations between the friction factor and Reynolds number have been developed [2,7,17]. The friction factor is then used to calculate the pressure drop across the spacer-filled channel. This approach is widely used to estimate the pressure drop across the channel in modeling and designing different membrane systems [18–23]. The empirical correlation approach provides a quick estimate of the average properties across a channel which is then used in macroscopic models to assess the membrane system performance [24]. However, this model is only suitable for investigating the performance of a module with the same spacer that was used to develop the empirical friction factor correlation. It is important to mention that there are many empirical correlations of the spacer friction factor vs. Reynolds number but there is no general correlation that could be used for spacers of different geometries, therefore, optimizing the membrane module geometry [25]. In addition, there is a need for a general pressure drop estimation model that suits any spacer characteristics.

Several studies used an alternative approach for studying a spacer-filled channel through computational fluid dynamics (CFD) to determine the mass transfer at a microscopic level [23,26–30]. Flow, concentration, and pressure distributions were investigated in a simplified 2D model using CFD models [31–34]. Different spacer filament geometries were compared, and the triangular filament cross-section was found to be the most effective at reducing concentration polarization [35]. However, a limitation of using 2D models is their inability to incorporate complex geometry features such as filament intersections. Due to the limitations of 2D models, 3D models are necessary for an accurate representation of channel hydrodynamics, thus, considering the effect of geometric features such as the angle of attack, filament intersection, and mesh angle [23,29,36–40]. Previous studies conducted 3D simulations either by using captured microscopic images of the spacer or by drawing cylindrical filaments in a crossing arrangement as the geometry of the computational domain. Picioreanu et al. [38] used a model based on microscopic images that captured the variation in filament diameter at the intersections. It was found that the pressure drop for the actual geometry was double that of the geometry based on crossing arrangements of cylindrical filaments. Although 3D simulations can be used to study spacer-filled channels more accurately compared to 2D simulations, it requires high computational power and can be time-consuming. In addition, commercially available spacers have more complex geometries compared to the geometry based on the crossing arrangement of the spacer filaments, due to the change in filament cross-section area at the filament crossing [38,41]. Thus, developing a different approach where realistic spacer geometries could be investigated is required.

Spacer geometry influences membrane fouling, mass transfer and pressure drop [27,42]. Membrane fouling can occur due to the presence of stagnant regions across the membrane resulting in the accumulation of microorganisms or salt residues hence reducing effective membrane area and increasing pressure drop [43,44]. Therefore, an optimal spacer design prevents the presence of stagnant regions and enhances the turbulence on the membrane surface to increase the mass transfer coefficient without a significant increase in pressure drop. For example, it was reported that pressure drop decreases with spacer porosity [45]. While the mass transfer coefficient increases with spacer thickness [29]. Also, it was found that spacers with diamond shape and large filament spacing have a better performance compared to other configurations tested [29]. Therefore, to design a membrane module that is both energy-efficient and cost-effective, spacer thickness, porosity, and geometrical structure should be optimized to eliminate stagnant regions and reduce pressure drop [15,44].

Experimental approaches have been initially employed to investigate the effect of spacer geometries on the mass transfer coefficient through a spacer-filled channel [2,3,7,8]. The empirical correlations derived from those experiments were used to estimate the mass transfer coefficient. However, the use of these correlations was limited as the experiments were conducted at velocities suitable for UF membranes [3,7,8] or using five spacers with different geometries [2]. More recent approaches to estimate the mass transfer coefficient include the use of CFD simulations to derive mathematical correlations that include detailed spacer geometry parameters [23,24,46–48]. Koutsou et al. [23,46] derived correlations based on using both experimental and CFD approaches to estimate pressure drop and Sherwood number in 3D spacer geometries. However, in their study, several correlations were derived for each spacer without including spacer geometry parameters. Furthermore, Gu et al. [24,47] developed new dimensionless correlations that account for different spacer geometries.

Although several studies have focused on studying the effect of spacer geometry on mass transfer coefficient, membrane fouling, and pressure drop, this study develops a new approach that estimates pressure drop only for different spacer geometries. The flow through the membrane spacer can be treated as flow through porous media, thus the Darcy–Forchheimer model can be utilized to determine the pressure drop through the spacer-filled channel. This model takes into consideration the viscous and inertial effects for the flow through the spacer, as well as the channel walls effect. However, the permeability and inertial coefficient are needed for this model, which can be either experimentally measured or estimated using correlations in the literature. The permeability of the porous media is related to its structure and geometrical characteristics. Several correlations for predicting permeability coefficient have been previously developed. The Kozeny–Carman equation describes a model for packed beds consisting of ellipsoids [49]. This model is suitable for flow parallel to cylindrical fibers or spherical packing beds. A limitation of the Kozeny–Carman is that it is only suitable for unidirectional flow along the fibers and is inaccurate for predicting transverse flow. Gutowski et al. [50] suggested using different values of the Kozeny constant in different directions. This modification, however, was inaccurate at low porosity values. Another correlation developed by Langmuir [51] provided an expression for the permeability coefficient across a fiber mat. The correlation assumed that the fibers will be parallel to the flow and evenly distributed and then introduced a numerical factor to account for fibers perpendicular to the flow or intercrossing fibers. Gebart [52] on the other hand

derived an equation for flow perpendicular to the fibers without considering flow parallel to the fibers. However, Chen [53] derived a permeability model for fluid flow in fibrous media for porosities higher than 0.75 which considers flow both parallel and perpendicular to the fibers of an orthogonal mesh configuration. Chen's model [53] is considered suitable for the flow characteristics that occur in the spacer-filled channel and will be utilized in the present study to estimate the permeability.

The objective of this study is to investigate the pressure drop across a spacer-filled channel by treating the spacer as a homogeneous and isotropic porous material and conducting CFD simulations. In this regard, the permeabilities of the porous material for different membrane spacers are estimated using Chen's [53] correlation calibrated by experimental data of spacers' pressure drop available in the literature. The calculated permeability coefficients are then used to estimate the pressure drop for different spacers using a Darcy–Forchheimer model. The critical Reynolds number for the transition between Darcy and non-Darcy flow is also estimated, thus the simple Darcy model could be used to estimate the pressure drop when the inertial effect is ignored. In addition, the effects of the spacer characteristics on the permeability coefficient are investigated.

2. Spacers porous media model

A three-dimensional model was developed to simulate the flow in a spacer-filled channel. The fluid flow in the spacer-filled channel is described as flow in a porous media, where the complex geometry of the membrane spacer is expressed by permeability and inertial coefficients. In this section, we describe the details of the permeability coefficient estimation, the model geometry used in the CFD simulations, the fluid flow model, boundary conditions, and the criteria to determine the transition from Darcy to non-Darcy flow. Fig. 1 shows schematic representations of 11 different spacer structures that are investigated in the present study. The experimental pressure drop across these spacers and the flow data were obtained by the study of Fárková [17]. The specifications of the spacers are represented by their thickness, porosity, diagonal lengths, and material as given in Table 1.

Flow-through porous media is described by the Darcy–Forchheimer equation as given by Eq. (1) for a 1-D isotropic porous medium.

$$\frac{\Delta P}{L} = \frac{\mu}{K} v + \frac{\rho F}{2} v^2 \tag{1}$$

The first term on the right-hand side of Eq. (1) represents the Darcy term with the permeability coefficient (K) which describes a linear relationship between the pressure drop and the superficial velocity. This relationship is only valid at relatively small velocities as the effect of drag forces is negligible. However, as the velocity increases, the transition to non-linear pressure drop with the superficial velocity occurs smoothly due to the added contribution of drag forces caused by spacer filaments. This is described by the second term in the equation's right-hand side and the inertial or Forchheimer coefficient (F). The transition is related to the appearance of the first eddies in the fluid flow. This change, however, is a transition to turbulent flow since the flow in the pores is still relatively small and can be described as laminar. There is no such sudden transition to non-linear pressure drop as the velocity increases.

The permeability of the porous media (K) is related to its structure and geometrical characteristics. Chen [53] derived a model for fluid flow in fibrous media for porosities higher than 0.75. This model considered fibers parallel and perpendicular to the flow in an orthogonal mesh configuration. The derived correlation for the permeability coefficient predicted by Chen [53] is given by Eq. (2).

$$K = \frac{\pi d_f^2 \ln\left(A / \sqrt{1-\varepsilon}\right)}{4B} \frac{\varepsilon}{1-\varepsilon} \tag{2}$$

where d_f represents the filament diameter, whereas ε represents porosity which characterizes void spaces in the spacer and can be expressed as the ratio of the volume of voids over the total volume. A and B are constants that

Table 1
Spacer specifications [17]

Spacer #	Spacer thickness b (mm)	Porosity ε	L_1 (mm)	L_2 (mm)	Material
1	1.00	0.78	4.75	3.15	Polypropylene
2	1.45	0.80	5.80	3.80	Polypropylene
3	2.00	0.87	16.40	8.10	Polypropylene
4	1.20	0.81	4.40	4.40	Polyethylene
5	1.40	0.89	7.00	7.00	Polyethylene
6	1.45	0.74	5.80	3.40	Polyethylene
7	1.45	0.88	8.20	8.20	Polyethylene
8	0.45	0.76	1.45	1.45	Polyester
9	0.50	0.87	1.05	1.05	Polypropylene
10	0.60	0.81	1.10	1.10	Polyamide
11	0.60	0.82	1.25	1.25	Polyamide

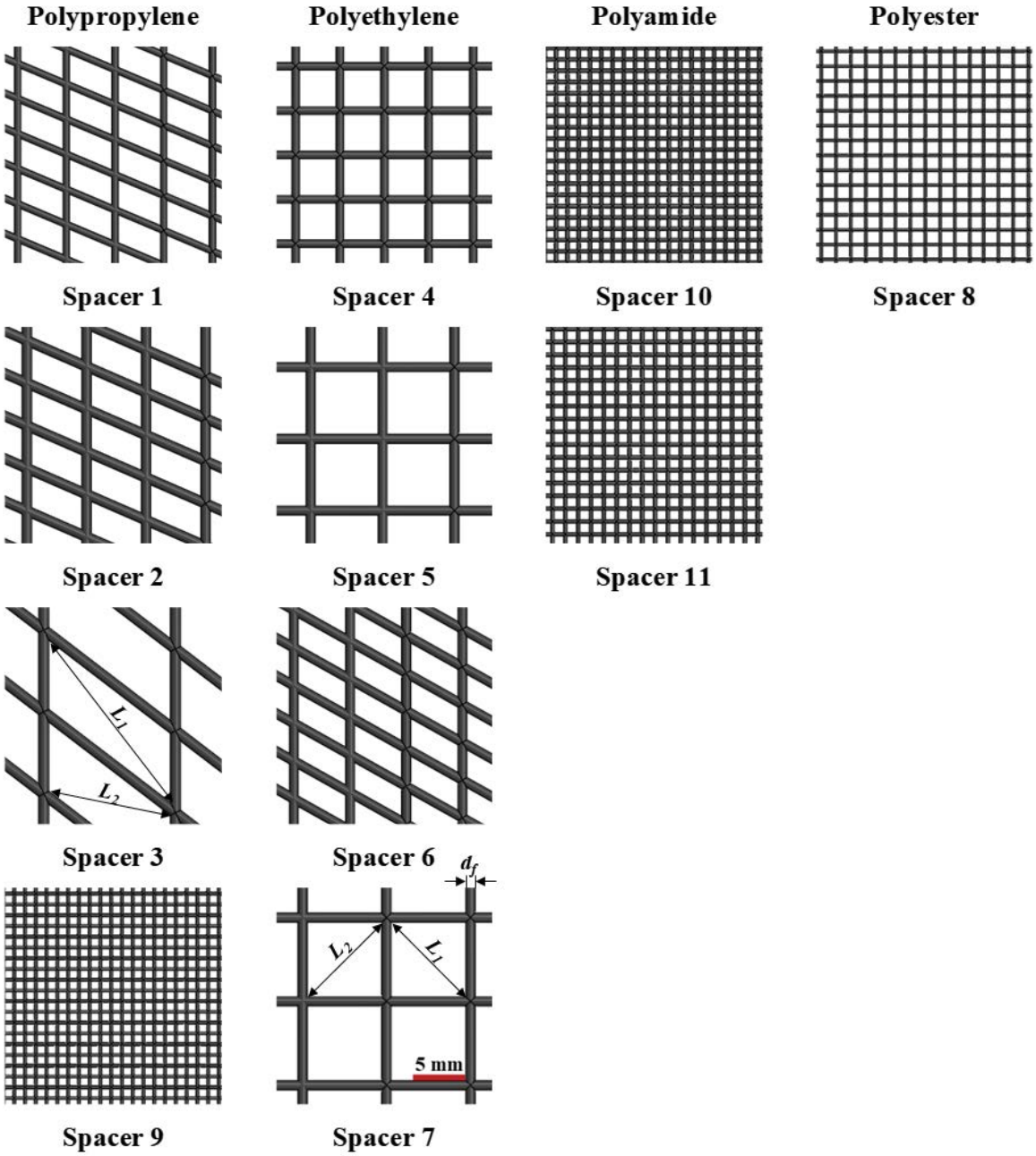

Fig. 1. Schematic representation of the investigated spacers.

should be determined based on experimental data. These constants were correlated in the present work for the 11 investigated spacers. The values for A and B were obtained using non-linear regression and are given as $A = 7.38 \times 10^9$ and $B = 1.35 \times 10^3$, respectively.

The critical Reynolds number for the transition from the Darcy to non-Darcy flow is calculated by plotting the Reynolds number (Re_K) against the friction factor (f_K) which are calculated by Eqs. (3) and (4).

$$f_K = \frac{\sqrt{K}}{L}\frac{\Delta P}{\rho v^2} \tag{3}$$

$$\mathrm{Re}_K = \frac{\rho v\sqrt{K}}{\mu} \tag{4}$$

In these equations, the characteristic length of f_K and Re_K is the square root of the permeability coefficient. At higher Reynolds numbers, the inertial term dominates over the Darcy term in pressure drop calculations and f_K becomes constant. Thus, the critical Re_K is estimated when f_K becomes constant [54]. Knowing this critical Reynolds number is important for distinguishing between Darcy and non-Darcy flow. In cases where the Re_K is lower than the critical value, it would be considered a Darcy flow

model, where the inertial coefficient (F) would be considered negligible and resulting in a faster CFD simulation and thus the pressure drop can be quickly estimated. However, if the Re_K is higher than the critical value, the model would be considered as a non-Darcy one and a Darcy–Forchheimer equation should be used, where an estimation of the inertial coefficient (F) would be required.

2.1. CFD simulations

CFD simulations for the flow-through spacer-filled channels were conducted using ANSYS-Fluent software. The geometry of the computational domain was selected based on the actual dimensions of each spacer in the experimental measurements conducted by the study of Fárková [17]. Fig. 2 shows the schematic and dimensions of the flow channel which has a rectangular cross-section with a length of L = 500 mm, a width of a = 90 mm, and a height that depends on each spacer thickness. The CFD simulations consider the channel wall effects as well as the spacer porous characteristics on the pressure drop.

A structured grid based on hexahedron cells was used to mesh the computational domain. Grid sensitivity analysis was performed to optimize the mesh density using mesh densities between 250,000 and 500,000 elements. An optimum mesh density of 450,000 elements was used in the simulations after which the variation in the pressure drop results was less than 1%. The boundary conditions of the computational domain are shown in Fig. 2 with velocity inlet boundary at the flow entry, pressure outlet boundary at the flow exit, and no-slip walls all around the flow channel. The inlet velocity was calculated from the Reynolds number value within the studied range. The flow direction was normal to the inlet and outlet faces. The domain was considered as a homogeneous porous media and the calculated permeability and inertial coefficients from the pressure drop data were used in the model parameters.

The fluid flow was assumed steady, incompressible, and Newtonian, which is governed by the continuity and Darcy–Forchheimer equations given by Eqs. (5) and (6).

$$\nabla V = 0 \tag{5}$$

$$\rho\left[\nabla\cdot\left(V\cdot V\right)\right] = -\nabla P + \mu\nabla^2 V - \frac{\mu}{K}V - \frac{\rho F}{2}V\left|V\right| \tag{6}$$

where V is the superficial velocity vector, P is the pressure, ρ is the density, and μ is the viscosity. The fluid used in the simulation was water with a density of 1,000 kg/m^3 and a dynamic viscosity of 8.9 × 10^{-4} Pa·s. The coupled algorithm was used for the pressure-velocity coupling, pressure interpolation was a second-order, and the second-order discretization scheme was used for the viscous terms of the governing equations. Convergence was assumed to be obtained when all the scaled residuals leveled off and reached 10^{-5}.

The flow rate was varied to investigate the performance of each spacer at different velocities. The Reynolds number was varied from 100 to 1,900 to match the experimental data by the study of Fárková [17]. Reynolds number was calculated based on the superficial velocity and hydraulic diameter as given by Eqs. (7) and (8) [17].

$$\mathrm{Re} = \frac{\rho v d_h}{\mu} \tag{7}$$

$$d_h = \frac{2ab\varepsilon}{a+b+4a\left(1-\varepsilon\right)} \tag{8}$$

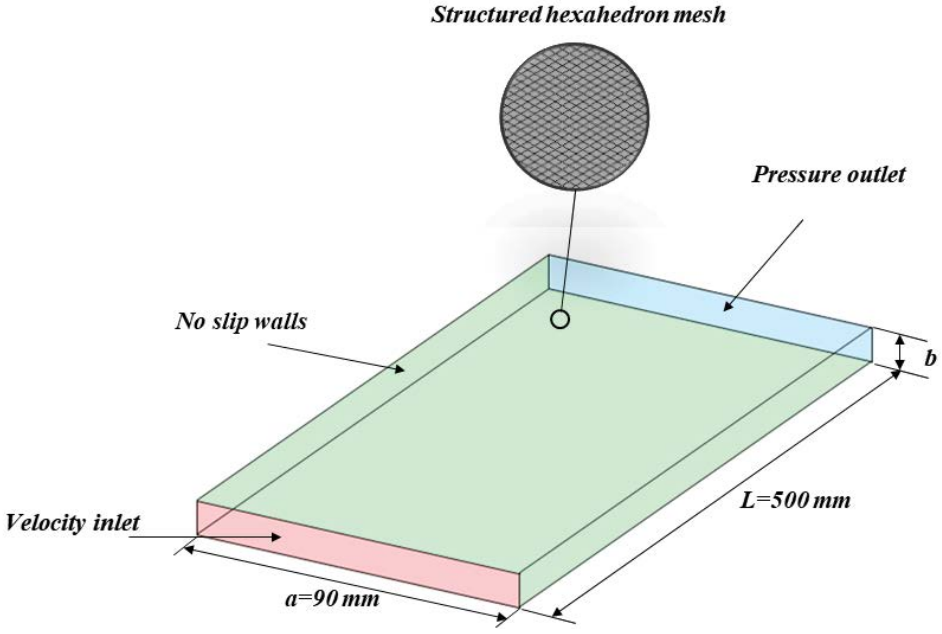

Fig. 2. Geometry and boundary conditions of the computational domain.

where *a* and *b* are the width and height of the flow channel. The pressure drop was calculated from the CFD simulation for every spacer at the studied range of Reynolds number and then validated with the experimental data [17].

3. Results and discussion

The pressure drop through a spacer-filled channel was investigated by treating the channel as a homogeneous porous media and conducting CFD simulations. In this section, a correlation for predicting the permeability coefficient, suitable for pressure drop calculation at Reynolds number lower than the critical Re_K, was generated and validated using experimental data. Additionally, critical Re_K for spacers with different thickness and porosity are calculated and compared to Re_K values for velocities within the common operating range. Furthermore, the effects of spacer specifications on the permeability are presented.

3.1. Permeability coefficient correlation

The permeability and inertial coefficients for 11 different spacers were calculated using the experimental data of Fárková [17]. These experiments were conducted by inserting different spacers in a channel cell that has a length of 500 mm and a width of 90 mm, whereas the height of the channel was adjusted to match the spacer thickness by adding a rubber seal below the spacer. The measured pressure drop ranged from 0.01 to 180 kPa corresponding to a flow velocity range of 0.05–2 m/s as shown in Fig. 3 for all spacers. It is important to mention that this measured velocity range is considered very high in the practical operation of membrane modules. For example, the recommended velocity in reverse osmosis (RO) spiral wound modules ranges from 0.07 to 0.16 m/s [55]. Comparing the pressure drop vs. velocity data to the Darcy–Forchheimer model [Eq. (1)], the permeability and inertial coefficients for each spacer were determined.

The pressure drop results from the CFD simulations and the experimental measurements for the 11 spacers investigated are given in Table 2. There is a good agreement between the calculated and measured pressure drop values with a maximum error of 8%. Thus, treating a membrane spacer as a porous media is a valid approach since the pressure drop prediction agrees well with the experimental measurements. However, the permeability and inertial coefficients of the spacer should be known to conduct CFD simulations. In addition, the critical Reynolds number for the transition between Darcy and non-Darcy flow should also be known. This in fact is a difficult step and there is no solid agreement in the literature on the value of the critical Reynolds number [56]. However, the approach discussed by Ward [57] is followed in the present work to estimate the critical Reynolds number for each spacer.

Fig. 4 shows the friction coefficient and Reynolds number as calculated by Eqs. (3) and (4) for the spacers of the maximum and minimum permeability. Following the approach discussed by Ward [57], the critical Reynolds number ranged from 50 to 140 for all spacers with the majority of spacers having a critical Reynolds number of about 100 as shown in Table 3. The Reynolds number corresponding to the recommended velocity range in the spacer-filled channels (0.07–0.16 m/s [55]) is highlighted in Fig. 4. The practical Reynolds number range overlaps with the

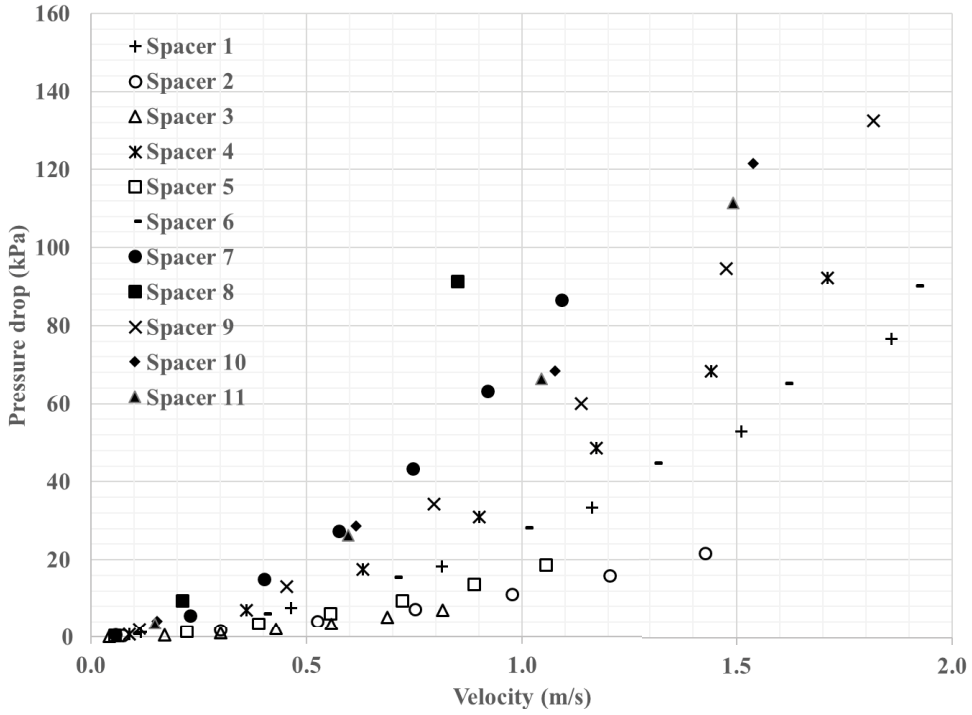

Fig. 3. The pressure drop dependence on velocity for different spacers from CFD results.

Table 2
Predicted and measured pressure drop of the 11 investigated spacers (experimental data from [17])

#	1			2			3			4			5			6		
Re	Pressure drop (Pa)		Error (%)	Pressure drop (Pa)		Error (%)	Pressure drop (Pa)		Error (%)	Pressure drop (Pa)		Error (%)	Pressure drop (Pa)		Error (%)	Pressure drop (Pa)		Error (%)
	Farkova	CFD		Farkova	CFD		Farkova	CFD		Farkova	CFD		Farkova	CFD		Farkova	CFD	
100	8.00×10^2	1.16×10^3	7.0%	2.24×10^2	2.46×10^2	2.7%	4.23×10^1	4.26×10^1	0.8%	6.57×10^2	6.53×10^2	0.7%	1.86×10^2	1.79×10^2	3.7%	6.15×10^2	6.16×10^2	0.1%
400	7.17×10^3	7.55×10^3	2.1%	1.73×10^3	1.74×10^3	0.0%	3.83×10^2	3.89×10^2	1.6%	6.71×10^3	7.03×10^3	4.7%	1.24×10^3	1.34×10^3	8.1%	6.09×10^3	5.96×10^3	2.1%
700	1.84×10^4	1.83×10^4	4.0%	4.36×10^3	4.03×10^3	0.7%	1.04×10^3	1.05×10^3	0.4%	1.73×10^4	1.75×10^4	1.0%	3.29×10^3	3.34×10^3	1.6%	1.59×10^4	1.52×10^4	4.0%
1,000	3.37×10^4	3.33×10^4	3.3%	7.86×10^3	7.15×10^3	2.1%	2.02×10^3	2.10×10^3	3.7%	3.16×10^4	3.09×10^4	2.0%	6.12×10^3	6.11×10^3	0.2%	2.92×10^4	2.80×10^4	4.0%
1,300	5.25×10^4	5.27×10^4	1.4%	1.21×10^4	1.11×10^4	2.0%	3.32×10^3	3.44×10^3	3.5%	4.92×10^4	4.86×10^4	1.3%	9.66×10^3	9.41×10^3	2.6%	4.57×10^4	4.46×10^4	2.4%
1,600	7.46×10^4	7.65×10^4	1.1%	1.71×10^4	1.59×10^4	1.6%	4.95×10^3	5.21×10^3	5.4%	6.99×10^4	6.84×10^4	2.1%	1.39×10^4	1.37×10^4	1.5%	6.52×10^4	6.50×10^4	0.4%
1,900	9.97×10^4	1.05×10^5	3.5%	2.27×10^4	2.16×10^4	0.3%	6.89×10^3	6.97×10^3	1.2%	9.34×10^4	9.22×10^4	1.2%	1.87×10^4	1.85×10^4	0.8%	8.75×10^4	8.99×10^4	2.8%

#	7			8			9			10			11		
Re	Pressure drop (Pa)		Error (%)	Pressure drop (Pa)		Error (%)	Pressure drop (Pa)		Error (%)	Pressure drop (Pa)		Error (%)	Pressure drop (Pa)		Error (%)
	Farkova	CFD		Farkova	CFD		Farkova	CFD		Farkova	CFD		Farkova	CFD	
100	5.44×10^2	5.56×10^2	2.2%	9.73×10^3	9.51×10^3	2.3%	2.15×10^3	2.12×10^3	1.1%	4.27×10^3	4.21×10^3	1.3%	3.41×10^3	3.49×10^3	2.3%
400	5.72×10^3	5.69×10^3	0.6%	9.66×10^4	9.13×10^4	5.5%	1.35×10^4	1.31×10^4	2.5%	2.92×10^4	2.86×10^4	2.0%	2.63×10^4	2.63×10^4	0.1%
700	1.51×10^4	1.50×10^4	0.2%	2.46×10^5	2.27×10^5	7.6%	3.45×10^4	3.43×10^4	0.5%	6.95×10^4	6.84×10^4	1.5%	6.52×10^4	6.63×10^4	1.7%
1,000	2.79×10^4	2.73×10^4	2.3%	4.46×10^5	4.42×10^5	1.0%	6.28×10^4	6.01×10^4	4.3%	1.21×10^5	1.22×10^5	0.6%	1.16×10^5	1.11×10^5	4.2%
1,300	4.40×10^4	4.34×10^4	1.4%	6.91×10^5	6.72×10^5	2.8%	9.75×10^4	9.47×10^4	2.9%	1.81×10^5	1.83×10^5	0.6%	1.78×10^5	1.73×10^5	2.9%
1,600	6.30×10^4	6.31×10^4	0.3%	9.78×10^5	9.75×10^5	0.2%	1.38×10^5	1.33×10^5	4.1%	2.50×10^5	2.46×10^5	1.8%	2.49×10^5	2.47×10^5	0.6%
1,900	8.48×10^4	8.66×10^4	2.1%	1.30×10^6	1.31×10^6	0.6%	1.84×10^5	1.80×10^5	2.4%	3.27×10^5	3.26×10^5	0.1%	3.29×10^5	3.38×10^5	2.9%

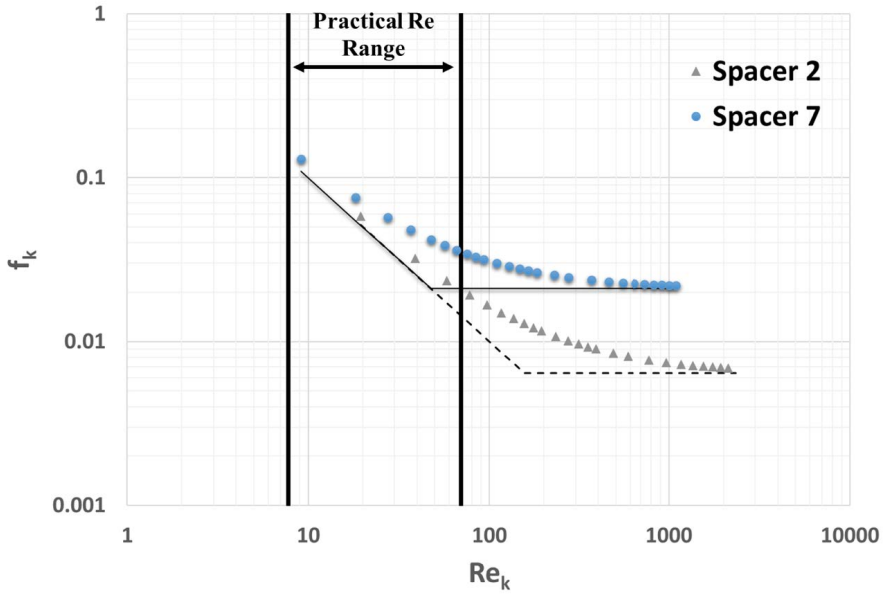

Fig. 4. The transition from Darcy to non-Darcy flow for spacers 2 and 7.

Table 3
Spacer permeability and inertial coefficients

Spacer #	Hydraulic diameter d_h (mm)	Equivalent diameter d_{eq} (mm)	Filament diameter* d_f (mm)	Permeability coefficient $K \times 10^8$ (m^2)	Inertial coefficient F (m^{-1})	Critical Re_K
1	0.86	3.09	0.67	6.30	71.3	112
2	1.33	3.75	0.97	15.10	33.0	140
3	2.33	9.20	1.33	64.85	38.6	60
4	1.11	3.51	0.80	3.32	89.1	101
5	1.80	5.59	0.93	13.76	53.1	97
6	0.99	3.54	0.97	7.14	84.1	115
7	1.74	6.54	0.97	4.51	254.9	48
8	0.47	1.16	0.30	0.97	282.9	100
9	0.88	0.84	0.33	2.28	117.0	102
10	0.65	0.88	0.40	1.56	114.4	140
11	0.67	1.00	0.40	1.89	135.3	120

*Assuming d_f is equal to two-third of the thickness (b).

critical Reynolds number (Re_K) range as shown in Fig. 4. However, in most cases, the practical Reynolds number is less than the critical Reynolds number (Re_K), and therefore, the flow in the spacers can be modeled with a Darcy model and the inertia effects can be ignored. Thus, developing a correlation for predicting the permeability of the spacers will be helpful to use the Darcy model and understand the effect of spacer characteristics on the pressure drop.

Chen's correlation [53] [Eq. (2)] is used to calculate the permeability of the spacers after calibrating the A and B constants in that equation. Fig. 5 shows the calculated permeability coefficient using [Eq. (2)] presented by the 3D surface as it changes with the filament diameter and porosity. In addition, the permeability coefficients as obtained from the experimental data are also shown in the same figure presented by the marked points. The correlation shows the same relationship between the porosity and filament diameter with the permeability coefficient. The obtained correlation has a mean deviation of 95%. The developed correlation for the permeability coefficient can be used in the Darcy equation to calculate the pressure drop in a spacer-filled channel at relatively low velocities which are commonly used in RO systems.

3.2. Permeability correlation validation

The proposed correlation for the permeability coefficient (Eq. 2) was validated using data obtained from [10] and [45] for different spacers. The reported spacers filament diameter and porosity were used to calculate the

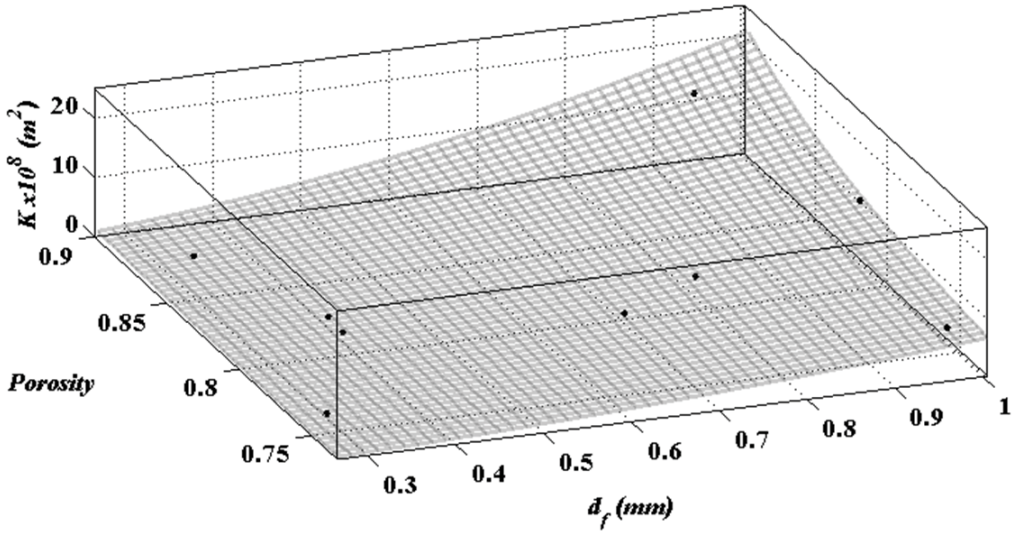

Fig. 5. The effect of spacer porosity and filament diameter on the spacer permeability.

permeability coefficient using Eq. (2). The Darcy model and CFD simulation were then used to compute the pressure drop. The spacer properties and calculated permeability coefficients are presented in Table 4. Three out of the six spacers in Siddiqui et al. [45] were excluded from the validation as their lowest Reynolds number was more than the critical one, thus the inertial effects cannot be ignored. However, for the low Reynolds number range, the predicted pressure drop was in good agreement with the experimental data with a maximum error of 14.5% as shown in Table 5. Thus, the proposed spacer permeability correlation and CFD approach are suitable for predicting pressure drop in a spacer-filled channel at Reynolds number lower than the critical one which is applicable in all membrane spacer applications.

3.3. Comparison with friction coefficient correlation

To further validate the pressure drop calculated using the proposed permeability correlation and CFD approach, the pressure drop was calculated using the friction coefficient correlation for spacer-filled channels developed by Schock and Miquel [2]. The friction coefficient is a function of Reynolds number and is given by:

$$f = 6.23 \cdot \mathrm{Re}^{-0.3} \quad \text{for} \quad 100 < \mathrm{Re} < 1{,}000 \tag{9}$$

The pressure drop can then be calculated from:

$$\Delta p = f \cdot \rho \cdot \frac{\upsilon^2}{2} \cdot \frac{L}{d_h} \tag{10}$$

where ρ is the density, v is the average velocity; L is the channel length, and d_h is the channel hydraulic diameter. The pressure drop was calculated using the Schock and Miquel's correlation [2] and compared with the experimental pressure drop and CFD results as shown in Table 5. For most of the spacers investigated, the calculated pressure drop was in good agreement with the experimental data. However, the polypropylene spacer had the highest error of 25.1%. This could be due to the error in the porosity measurement, as a 5% deviation in porosity was previously reported to lead to a 30% error in pressure drop [45]. The average error in pressure drop values calculated using the CFD approach was 5.7% while the average error in pressure drop values calculated using Schock and Miquel correlation was 10% as shown in Table 5.

3.4. Spacer geometry effect on permeability

Spacer characteristics have a great impact on the permeability and hence pressure drop. Although Chen's [53] correlation included the porosity and the filament diameter as parameters to determine the permeability, it was

Table 4
Spacer properties and permeability coefficient used in correlation validation

Spacer name	Porosity ε	Filament diameter d_f (mm)	Permeability coefficient $K \times 10^8$ (m^2)	Reference
Polypropylene	0.87	0.760	5.34	[10]
DOW	0.88	0.833	6.78	[45]
HYD	0.89	0.839	8.06	[45]
LXS-ASD	0.89	0.857	7.91	[45]

Table 5
Comparison between pressure drop data using the numerical model, Schock and Miquel correlation [2], and experimental data [10,45]

Spacer name	Flow rate (L/h)	Pressure drop (Pa)			Error (%)		Reference
		Experimental	CFD	Schock and Miquel [2]	CFD	Schock and Miquel [2]	
Polypropylene	0.13	227	230	170	–1.3	–25.1	[10]
	0.22	387	331	297	14.5	–23.2	
DOW	2	88	81	80	8	–9.5	[45]
	4	285	292	259	–2.5	–9.2	
HYD	2	77	71	77	7.8	0.0	[45]
	4	285	257	250	9.8	–12.2	
LXS-ASD	2	150	145	164	3.3	9.4	[45]

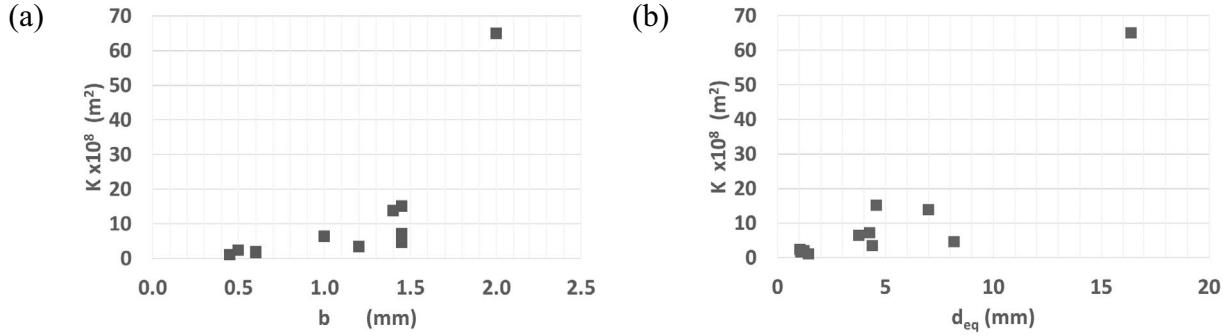

Fig. 6. The effect of spacer properties (a) spacer thickness and (b) equivalent diameter on permeability.

noticed that other spacer geometrical properties influence the permeability too. The permeability is highly reliant on the thickness and equivalent diameter of the spacer as well as the porosity and filament diameter, as shown in Fig. 6. The equivalent diameter was calculated by converting the open space area into a circle to examine the effect of the spacer diagonal lengths. It is shown in Fig. 6 that the permeability increases significantly with a higher thickness and a larger equivalent diameter. This resulted in a lower pressure drop which is expected with the presence of larger voids, comparable to the pressure drop across an empty channel. The effect of the other geometrical parameters of the spacer on permeability suggests that a more detailed correlation for permeability estimation is needed.

4. Conclusion

A new approach to calculate the pressure drop across a spacer-filled channel is presented. The approach treats the spacer-filled channel as a homogeneous and isotropic porous medium and uses the Darcy–Forchheimer model and CFD analysis to calculate the pressure drop. The permeability coefficient is first calculated using a modified version of Chen's correlation (Eq. 2) which estimates the spacer permeability based on its filament diameter and porosity. The permeability and inertial coefficients of the Darcy–Forchheimer model were determined using experimental data in the literature to determine the transition between Darcy and non-Darcy flow. The transition was identified and found that within the common flow velocities in spacers, the flow should be considered as a Darcy flow where the inertial effects could be ignored without affecting the pressure drop calculation. A good agreement was found between the experimental data and the calculated pressure drop values with a mean error of 5.7%. Therefore, the CFD approach and permeability coefficient correlation used in this study can be used for predicting pressure drop in a spacer-filled channel for membrane modules at Reynolds number less than the critical one. Finally, it was found that the thickness and equivalent diameter of the spacer also affect its permeability. This suggests that a more detailed permeability estimation correlation for spacers should be considered in future investigations.

Acknowledgment

The authors would like to thank the Natural Sciences and Engineering Research Council of Canada (NSERC–Grant #401366) for the funding support provided for this research.

Symbols

A	—	Constant in Eq. (2), –
a	—	Channel width, m
B	—	Constant in Eq. (2), –
b	—	Spacer thickness/channel height, m

d_{eq}	—	Equivalent diameter, m
d_f	—	Filament diameter, m
d_h	—	Hydraulic diameter, m
F	—	Inertial coefficient, m^{-1}
f	—	Friction coefficient, –
K	—	Permeability coefficient, m^2
L	—	Diagonal/channel length, m
P	—	Pressure, Pa
Re	—	Reynolds number, –
V	—	Velocity vector, m/s
v	—	Velocity, m/s

Greek

ε	—	Porosity, –
μ	—	Viscosity, kg/m s
ρ	—	Density, kg/m^3

References

[1] C.C. Zimmerer, V. Kottke, Effects of spacer geometry on pressure drop, mass transfer, mixing behavior, and residence time distribution, Desalination, 104 (1996) 129–134.

[2] G. Schock, A. Miquel, Mass transfer and pressure loss in spiral wound modules, Desalination, 64 (1987) 339–352.

[3] A.R. da Costa, A.G. Fane, Net-type spacers: effect of configuration on fluid flow path and ultrafiltration flux, Ind. Eng. Chem. Res., 33 (1994) 1845–1851.

[4] O. Kavianipour, G.D. Ingram, H.B. Vuthaluru, Studies into the mass transfer and energy consumption of commercial feed spacers for RO membrane modules using CFD: effectiveness of performance measures, Chem. Eng. Res. Des., 141 (2019) 328–338.

[5] F. Li, W. Meindersma, A.B. de Haan, T. Reith, Optimization of commercial net spacers in spiral wound membrane modules, J. Membr. Sci., 208 (2002) 289–302.

[6] N. Sreedhar, N. Thomas, O. Al-Ketan, R. Rowshan, H. Hernandez, R.K. Abu Al-Rub, H.A. Arafat, 3D printed feed spacers based on triply periodic minimal surfaces for flux enhancement and biofouling mitigation in RO and UF, Desalination, 425 (2018) 12–21.

[7] A.R. Da Costa; A.G. Fane; D.E. Wiley, Spacer characterization and pressure drop modelling in spacer-filled channels for ultrafiltration, J. Membr. Sci., 87 (1994) 79–98.

[8] A.R. Da Costa, A.G. Fane, C.J.D. Fell, A.C.M. Franken, Optimal channel spacer design for ultrafiltration, J. Membr. Sci., 62 (1991) 275–291.

[9] D.G. Thomas, Forced convection mass transfer in hyper-filtration at high fluxes, Ind. Eng. Chem. Fundam., 12 (1973) 396–405.

[10] A.H. Haidari, S.G.J. Heijman, W.G.J. van der Meer, Visualization of hydraulic conditions inside the feed channel of reverse osmosis: a practical comparison of velocity between empty and spacer-filled channel, Water Res., 106 (2016) 232–241.

[11] O. Kavianipour, G.D. Ingram, H.B. Vuthaluru, Investigation into the effectiveness of feed spacer configurations for reverse osmosis membrane modules using computational fluid dynamics, J. Membr. Sci., 526 (2017) 156–171.

[12] S. Kerdi, A. Qamar, J.S. Vrouwenvelder, N. Ghaffour, Fouling resilient perforated feed spacers for membrane filtration, Water Res., 140 (2018) 211–219.

[13] J. Schwinge, P.R. Neal, D.E. Wiley, D.F. Fletcher, A.G. Fane, Spiral wound modules and spacers: review and analysis, J. Membr. Sci., 242 (2004) 129–153.

[14] A. Ruiz-García, I. de la N. Pestana, Feed spacer geometries and permeability coefficients. Effect on the performance in BWRO spiral-wound membrane modules, Water, 11 (2019) 152, doi: 10.3390/w11010152.

[15] A.H. Haidari, S.G.J. Heijman, W.G.J. van der Meer, Optimal design of spacers in reverse osmosis, Sep. Purif. Technol., 192 (2018) 441–456.

[16] J. Schwinge, D.E. Wiley, D.F. Fletcher, Simulation of the flow around spacer filaments between channel walls. 2. Mass-transfer enhancement, Ind. Eng. Chem. Res., 41 (2002) 4879–4888.

[17] J. Fárková, The pressure drop in membrane module with spacers, J. Membr. Sci., 64 (1991) 103–111.

[18] Q. She, D. Hou, J. Liu, K. Hai, C.Y. Tang, Effect of feed spacer induced membrane deformation on the performance of pressure retarded osmosis (PRO): implications for PRO process operation, J. Membr. Sci., 445 (2013) 170–182.

[19] A. Sagiv, W. Xu, P.D. Christo, Y. Cohen, R. Semiat, Evaluation of osmotic energy extraction via FEM modeling and exploration of PRO operational parameter space, Desalination, 401 (2017) 120–133.

[20] J. Maisonneuve, P. Pillay, C.B. Laflamme, Pressure-retarded osmotic power system model considering non-ideal effects, Renewable Energy, 75 (2015) 416–424.

[21] Y. Roy, M.H. Sharqawy, J.H. Lienhard V, Modeling of flat-sheet and spiral-wound nanofiltration configurations and its application in seawater nanofiltration, J. Membr. Sci., 493 (2015) 360–372.

[22] B. Abdelkader, M.H. Sharqawy, Temperature effects and entropy generation of pressure retarded osmosis process, Entropy, 21 (2019) 1158, doi: 10.3390/e21121158.

[23] C.P. Koutsou, S.G. Yiantsios, A.J. Karabelas, A numerical and experimental study of mass transfer in spacer-filled channels: Effects of spacer geometrical characteristics and Schmidt number, J. Membr. Sci., 326 (2009) 234–251.

[24] B. Gu, C.S. Adjiman, X.Y. Xu, The effect of feed spacer geometry on membrane performance and concentration polarisation based on 3D CFD simulations, J. Membr. Sci., 527 (2017) 78–91.

[25] V. Geraldes, V. Semião, M.N. De Pinho, Flow management in nanofiltration spiral wound modules with ladder-type spacers, J. Membr. Sci., 203 (2002) 87–102.

[26] J.L.C. Santos, V. Geraldes, S. Velizarov, J.G. Crespo, Investigation of flow patterns and mass transfer in membrane module channels filled with flow-aligned spacers using computational fluid dynamics (CFD), J. Membr. Sci., 305 (2007) 103–117.

[27] G.A. Fimbres-Weihs, D.E. Wiley, Review of 3D CFD modeling of flow and mass transfer in narrow spacer-filled channels in membrane modules, Chem. Eng. Process. Process Intensif., 49 (2010) 759–781.

[28] C.P. Koutsou, A.J. Karabelas, Shear stresses and mass transfer at the base of a stirred filtration cell and corresponding conditions in narrow channels with spacers, J. Membr. Sci., 399–400 (2012) 60–72.

[29] M. Shakaib, S.M.F. Hasani, M. Mahmood, CFD modeling for flow and mass transfer in spacer-obstructed membrane feed channels, J. Membr. Sci., 326 (2009) 270–284.

[30] K.Y. Toh, Y.Y. Liang, W.J. Lau, D.F. Fletcher, CFD study of the effect of perforated spacer on pressure loss and mass transfer in spacer-filled membrane channels, Chem. Eng. Sci., 222 (2020) 115704, doi: 10.1016/j.ces.2020.115704.

[31] G.A. Fimbres-Weihs, D.E. Wiley, Numerical study of two-dimensional multi-layer spacer designs for minimum drag and maximum mass transfer, J. Membr. Sci., 325 (2008) 809–822.

[32] R.E. Ahmad, A.H. Earle, P. Hugues, R. Maharaj, Landslide damage to the Boar River water supply pipeline, Bromley Hill, Jamaica: case study of a landslide caused by Hurricane Gilbert (1988), Int. J. Rock Mech. Min. Sci. Geomech. Abstr., 31 (2006) A46.

[33] S. Wardeh, H.P. Morvan, CFD simulations of flow and concentration polarization in spacer-filled channels for application to water desalination, Chem. Eng. Res. Des., 86 (2008) 1107–1116.

[34] J. Schwinge, D.E. Wiley, D.F. Fletcher, A CFD study of unsteady flow in narrow spacer-filled channels for spiral-wound membrane modules, Desalination, 146 (2002) 195–201.

[35] A.L. Ahmad, K.K. Lau, M.Z. Abu Bakar, Impact of different spacer filament geometries on concentration polarization

control in narrow membrane channel, J. Membr. Sci., 262 (2005) 138–152.
[36] V.V. Ranade, A. Kumar, Fluid dynamics of spacer filled rectangular and curvilinear channels, J. Membr. Sci., 271 (2006) 1–15.
[37] A. Saeed, R. Vuthaluru, Y. Yang, H.B. Vuthaluru, Effect of feed spacer arrangement on flow dynamics through spacer filled membranes, Desalination, 285 (2012) 163–169.
[38] C. Picioreanu, J.S. Vrouwenvelder, M.C.M. van Loosdrecht, Three-dimensional modeling of biofouling and fluid dynamics in feed spacer channels of membrane devices, J. Membr. Sci., 345 (2009) 340–354.
[39] Y.L. Li, K.L. Tung, CFD simulation of fluid flow through spacer-filled membrane module: selecting suitable cell types for periodic boundary conditions, Desalination, 233 (2008) 351–358.
[40] Y.L. Li, K.L. Tung, M.Y. Lu, S.H. Huang, Mitigating the curvature effect of the spacer-filled channel in a spiral-wound membrane module, J. Membr. Sci., 329 (2009) 106–118.
[41] J.S. Vrouwenvelder, C. Picioreanu, J.C. Kruithof, M.C.M. van Loosdrecht, Biofouling in spiral wound membrane systems: three-dimensional CFD model based evaluation of experimental data, J. Membr. Sci., 346 (2010) 71–85.
[42] I. El Mokhtar, L. Gurreri, A. Tamburini, A. Cipollina, M. Ciofalo, T. Bouguecha, G. Micale, CFD prediction of flow, heat and mass transfer in woven spacer-filled channels for membrane processes, Int. J. Heat Mass Transfer, 173 (2021) 121246, doi: 10.1016/j.ijheatmasstransfer.2021.121246.
[43] S. Muztuza, Y. Kim, A. Qamar, G. Naidu, S. Phuntsho, N. Ghaffour, J.S. Vrouwenvelder, H. Kyong, Dynamic feed spacer for fouling minimization in forward osmosis process, Desalination, 515 (2021) 115198, doi: 10.1016/j.desal.2021.115198.
[44] H.S. Abid, D.J. Johnsona, R. Hashaikeh, N. Hilal, A review of efforts to reduce membrane fouling by control of feed spacer characteristics, Desalination, 420 (2017) 384–402.
[45] A. Siddiqui, S. Lehmann, V. Haaksman, J. Ogier, C. Schellenberg, M.C.M. van Loosdrecht, J.C. Kruithof, J.S. Vrouwenvelder, Porosity of spacer-filled channels in spiral-wound membrane systems: quantification methods and impact on hydraulic characterization, Water Res., 119 (2017) 304–311.
[46] C.P. Koutsou, S.G. Yiantsios, A.J. Karabelas, Direct numerical simulation of flow in spacer-filled channels: effect of spacer geometrical characteristics, J. Membr. Sci., 291 (2007) 53–69.
[47] B. Gu, C.S. Adjiman, X.Y. Xu, Correlations for concentration polarization and pressure drop in spacer-filled RO membrane modules based on CFD simulations, Membranes, 11 (2021) 338, doi: 10.3390/membranes11050338.
[48] Y.Y. Liang, K.Y. Toh, G.A. Fimbres Weihs, 3D CFD study of the effect of multi-layer spacers on membrane performance under steady flow, J. Membr. Sci., 580 (2019) 256–267.
[49] P.C. Carman, Fluid flow through granular beds, Trans. Int. Chem. Eng., 15 (1937) 150–166.
[50] T.G. Gutowski, T. Morigaki, Z. Cai., The consolidation of laminate composites, J. Compos. Mater., 21 (1987) 172–188.
[51] W.E. Ranz, The Role of Particle Diffusion and Interception in Aerosols Filtration, Vol. 1009, University of Illinois, Engineering Experiment Station, 1953.
[52] B.R. Gebart, Permeability of unidirectional reinforcements for RTM, J. Compos. Mater., 26 (1992) 1100–1133.
[53] C.Y. Chen, Filtration of aerosols by fibrous media, Chem. Rev., 55 (1955) 595–623.
[54] D.A. Nield, A. Bejan, Convection in Porous Media, 5th ed., New York, Springer, 2017.
[55] S.S. Bucs, R. Valladares Linares, J.O. Marston, A.I. Radu, J.S. Vrouwenvelder, C. Picioreanu, Experimental and numerical characterization of the water flow in spacer-filled channels of spiral-wound membranes, Water Res., 87 (2015) 299–310.
[56] Z. Zeng, R. Grigg, A criterion for non-Darcy flow in porous media, Trans. Porous Media, 63 (2006) 57–69.
[57] J.C. Ward, Turbulent flow in porous media, J. Hydraul. Div., 90 (1964) 1–12.